^{68}Ga-FAPI PET/CT as an Alternative to ^{18}F-FDG PET/CT in the Imaging of Invasive Lobular Breast Carcinoma

Ertan Sahin[1], Tulay Kus[2], Alper Aytekin[3], Evren Uzun[4], Umut Elboga[1], Latif Yilmaz[3], Yusuf B. Cayirli[1], Merve Okuyan[1], Vuslat Cimen[1], and Ufuk Cimen[1]

[1]Department of Nuclear Medicine, Gaziantep University, Gaziantep, Turkey; [2]Department of Medical Oncology, Gaziantep University, Gaziantep, Turkey; [3]Department of General Surgery, Gaziantep University, Gaziantep, Turkey; and [4]Department of Pathology, Gaziantep University, Gaziantep, Turkey

Accurate staging of invasive lobular carcinoma (ILC), a subtype of breast cancer, is vital for effective clinical management. Although ^{18}F-FDG PET/CT is a commonly used tool, its efficacy varies across different histologic subtypes. To mitigate this challenge, our investigation delves into the potential utility of ^{68}Ga-fibroblast activation protein inhibitor (FAPI) PET/CT as an alternative for staging ILC, aiming to address a significant research gap using a more expansive patient cohort than the smaller samples commonly found in the existing literature. **Methods:** In this retrospective analysis, women diagnosed with primary ILC of the breast underwent both ^{18}F-FDG PET/CT and ^{68}Ga-FAPI PET/CT. Both modalities were compared across all lesion locations with the used reference standard. The interval between scans was 1 wk, without any intervening treatments. Lesions were categorized visually, and tracer activity was analyzed using SUV_{max}, tumor-to-background uptake ratio, and uptake ratios. Both modalities were compared across various parameters, and statistical analysis was performed using SPSS 22.0. A P value of less than 0.05 was chosen to determine statistical significance. **Results:** The study included 23 female ILC patients (mean age, 51 y) with hormone-positive, human epidermal growth factor receptor type 2–negative tumors. Most (65%) had the luminal A subtype. ^{68}Ga-FAPI PET/CT outperformed ^{18}F-FDG PET/CT, with higher tumoral activity and tumor-to-background uptake ratios ($P < 0.001$). Primary tumors showed significantly increased uptake with ^{68}Ga-FAPI PET/CT ($P < 0.001$), detecting additional foci, including multicentric cancer. Axillary lymph node metastases were more frequent and had higher uptake values with ^{68}Ga-FAPI PET/CT ($P = 0.012$). Moreover, ^{68}Ga-FAPI PET/CT identified more lesions, including bone and liver metastases. Pathologic features did not significantly correlate with imaging modalities, but a positive correlation was observed between peritumoral lymphocyte ratio and ^{68}Ga-FAPI PET/CT–to–^{18}F-FDG PET/CT uptake ratios ($P = 0.026$). **Conclusion:** This study underscores ^{68}Ga-FAPI PET/CT's superiority over ^{18}F-FDG PET/CT for ILC. ^{68}Ga-FAPI PET/CT excels in detecting primary breast masses, axillary lymph nodes, and distant metastases; can complement ^{18}F-FDG PET/CT in ILC; and holds potential as an alternative imaging method in future studies.

Key Words: ^{68}Ga-FAPI-PET/CT; ^{18}F-FDG PET/CT; lobular breast carcinoma

J Nucl Med 2024; 65:512–519
DOI: 10.2967/jnumed.123.266798

Breast cancer is the most common cancer in women worldwide, comprising 25% of female cancer cases (*1*). Invasive lobular carcinoma (ILC) accounts for about 10% of all invasive breast cancer cases (*2*,*3*). Precise clinical staging is crucial for treatment decisions and prognosis (*4*,*5*).

Staging methods combine systemic and local assessments. Systemic staging uses various diagnostic tools such as bone scans, abdominal CT/MRI, thoracic CT, and ^{18}F-FDG PET. Local disease extent is determined with mammography, ultrasound, and breast MRI (*6*). ^{18}F-FDG PET/CT, crucial for breast cancer management, aids in initial staging, restaging, treatment response evaluation, and recurrence detection (*7*).

The utility of ^{18}F-FDG PET/CT, however, exhibits variability among histologic subtypes, particularly in the case of ductal and lobular breast cancers. The inherent challenges of identifying ILC with ^{18}F-FDG PET/CT stem from distinct molecular and pathologic features, including lower cellular density, receptor expression, and metastatic patterns (*2*,*3*); furthermore, primary and metastatic ILC is less ^{18}F-FDG–avid than invasive ductal cancer (IDC), leading to the weakness of ^{18}F-FDG PET for ILC (*8*,*9*). Additionally, factors such as small tumor size (<1 cm), in situ carcinomas, micrometastases, low-grade tumors, and benign pathologies can compromise the sensitivity and specificity of ^{18}F-FDG PET/CT in breast cancer (*10*–*12*).

To address limitations, prior research explored alternatives such as ^{18}F-fluoroestradiol, especially for ILC (*13*,*14*). Recently, a new radiopharmaceutical targeting fibroblast activation protein (FAP) has gained attention for tumor diagnosis and staging. FAP, highly expressed in cancer-associated fibroblasts (CAFs) (*15*–*18*), shows promise in PET studies, especially in combination with ^{68}Ga, due to favorable pharmacokinetics and high tumor background activity (*19*–*22*).

The unique role of the tumor stroma and the abundant stromal expression of FAP in primary breast cancer suggest a potential for high accuracy in FAPI-directed imaging (*23*,*24*). Recent studies have emerged comparing ^{18}F-FDG PET/CT and ^{68}Ga-FAPI PET/CT in breast cancer (*25*–*27*). Recent studies, including one by Eshet et al., compare ^{18}F-FDG PET/CT and ^{68}Ga-FAPI PET/CT in breast cancer, specifically in patients with ILC, albeit within a limited cohort (*25*–*27*).

Motivated by the paucity of literature on this subject, this study aimed to evaluate whether ^{68}Ga-FAPI PET/CT outperforms ^{18}F-FDG PET/CT in the context of ILC, with a focus on a larger patient cohort.

Received Oct. 4, 2023; revision accepted Jan. 11, 2024.
For correspondence or reprints, contact Ertan Sahin (er_ahin@yahoo.com).
Published online Mar. 14, 2024.

MATERIALS AND METHODS

Patient Selection and Evaluation

This study, approved by the Institutional Clinical Research Ethics Committee, included 23 women with ILC. They underwent ^{18}F-FDG PET/CT and ^{68}Ga-FAPI PET/CT for staging before systemic chemotherapy or surgery (Fig. 1). Secondary confirmation methods, such as bone scintigraphy–radiologic imaging or repeat ^{68}Ga-FAPI PET/CT, were routinely used because of potential limitations in ^{18}F-FDG PET/CT for the ILC subtype. The interval between scans was limited to 1 wk, with no intervening treatments. Eligible patients were 18 y old or older, with no recent systemic treatment or radiotherapy and a confirmed diagnosis of ILC. All provided written informed consent. Exclusions comprised men, individuals under 18 y old, secondary malignancy, severe hepatic–renal impairment, pregnancy, and breastfeeding.

Patient Preparation and PET/CT Imaging Protocols

^{18}F-FDG PET/CT. The patients underwent a standardized preparation regimen before the ^{18}F-FDG PET/CT imaging session, including a 12-h fast. Blood glucose levels had to be below 150 mg/dL. A 5 MBq/kg dose of ^{18}F-FDG was administered intravenously. Sixty minutes later, imaging was conducted using a Discovery IQ PET/CT device (GE Healthcare), scanning from the vertex to the mid femur.

^{68}Ga-FAPI PET/CT. ^{68}Ga-FAPI was synthesized and labeled using the Modular Lab-Easy system (Eckert & Ziegler) in a modular laboratory at our center, following a procedure akin to prior studies (*18*,*19*). Quality control assessments using thin-layer chromatography and high-performance liquid chromatography affirmed a radiochemical purity exceeding 98%. Subsequently, a 2–3 MBq/kg dose of synthesized ^{68}Ga-FAPI was intravenously injected into patients. Forty-five minutes later, PET/CT imaging was conducted using the Discovery IQ PET/CT device, covering the vertex to the mid femur.

Pathologic Evaluation

In the pathologic assessment, specimens obtained through Tru-Cut (Merit Medical) biopsy and excision were confirmed as malignant on the basis of criteria such as anaplasia, absence of myoepithelial cells, and the presence of mitosis or necrosis. Cases were evaluated for histologic tumor type, presence of ductal or lobular carcinoma in situ, nuclear grade, tumor-to-stroma ratio, and lymphocyte density and were graded using the Nottingham histologic scoring system.

Immunohistochemistry on tissue sections assessed estrogen receptor, progesterone receptor, Ki-67, and human epidermal growth factor receptor 2/neu expression. Estrogen receptor and progesterone receptor were evaluated in decimal percentiles, with staining intensity graded as weak, moderate, or strong. Invasive carcinomas with estrogen receptor and progesterone receptor between 1% and 10% were considered low positive, less than 10% staining was negative (score 1), and intense staining in more than 10% was positive (score 3). Human epidermal growth factor receptor 2/neu–equivocal cases were verified with human epidermal growth factor receptor 2 silver in situ hybridization, categorizing tumors into 5 molecular subtypes based on immunohistochemical results.

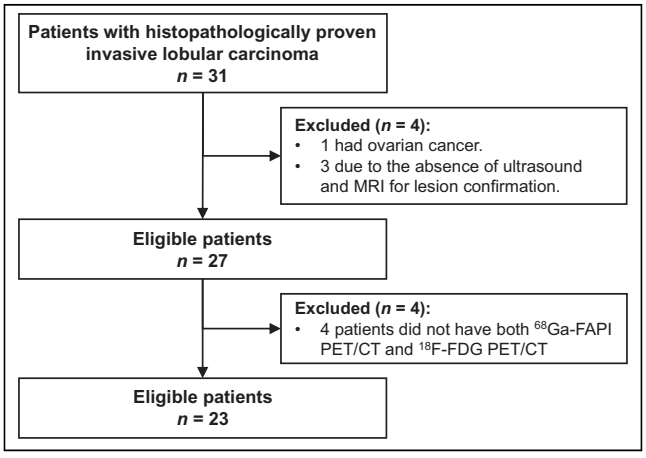

FIGURE 1. Descriptive flowchart of study.

Evaluation of Images and Patient-Lesion Analysis

Two experienced nuclear medicine physicians meticulously reviewed the PET/CT images, categorizing lesions as positive if detected by at least 1 specialist and negative if not detected. Classification of lesions without histopathologic confirmation was based on imaging methods (ultrasound, mammography, CT, MRI) and clinical findings. Histopathologic examination was conducted for 5 axillary lymph nodes in metastatic lesions, whereas decisions for other sites relied on imaging methods and clinical data.

For both PET/CT methods, areas with higher uptake than background were assessed as positive; findings from other modalities were also considered in the assessment. Images in axial, coronal, and sagittal planes were available for review. Semiquantitative analysis used SUV_{max}, with volumes of interest around primary breast lesions in 3 planes for both scans. SUV_{max} for primary lesions and metastases was determined, and radiopharmaceutical uptake exceeding background was quantified using SUV_{max} and tumor-to-background uptake ratio. The obtained imaging findings from both PET/CT methods were compared on both a patient basis and a lesion basis for further analysis and interpretation. Staging was done according to the method of the American Joint Committee on Cancer (*28*).

Reference Standard

All patients who were evaluated had been discussed in the multidisciplinary council for breast cancer before the data were scanned retrospectively. This council includes departments such as medical oncology, radiation oncology, general surgery, medical pathology, radiology, and nuclear medicine. Additional foci observed in PET/CT imaging for multifocal or multicentric primary malignancies, which had not undergone histopathologic testing, were further assessed using previous mammography and MRI results to determine malignancy. If there was no histopathologic evidence, regional lymph nodes observed in PET/CT imaging were correlated with previous ultrasonographic and MRI results, taking into account their molecular and morphologic characteristics depicted in the PET/CT imaging.

Moreover, the molecular and morphologic properties of distant lymph node, visceral, and bone involvement reported through PET/CT imaging were evaluated alongside routinely performed conventional imaging, as for breast lesions and regional lymph nodes. Finally, alignment of the latest decisions with the conclusions documented by the multidisciplinary council was ensured through consensus, also considering treatment response evaluations across all lesion sites during follow-up periods. The median follow-up was 4 mo (range, 3–6 mo). Consequently, the integration of multiple diagnostic modalities and multidisciplinary discussions formed a robustly constructed reference standard.

Statistical Analysis

The study data underwent descriptive statistical analysis, presenting numeric variables as mean and SD and categoric variables through frequency and percentage analysis. The normality and homogeneity of variance were tested using the Shapiro–Wilk and Levene tests, respectively. For nonnormally distributed dependent variables, the Wilcoxon signed-rank test was used, whereas the Mann–Whitney *U* test compared nonnormally distributed independent variables. Continuous variables were evaluated with the Pearson correlation test, and categoric

variables with the Spearman correlation test. SPSS 22.0 software was used for statistical analyses, with the significance level set at a P value of less than 0.05.

RESULTS

Patient Demographics and Tumor Characteristics

In total, 23 women with ILC were enrolled in this study. Their mean age was 51 y (range, 37–79 y), with 8 being premenopausal. Before undergoing PET/CT, 4 patients had undergone breast surgery. Additionally, 2 patients had bilateral breast cancer involvement (Fig. 2). The pathologic and clinical characteristics of the patients are summarized in Table 1.

Comparative PET/CT Analysis

The study revealed that ^{68}Ga-FAPI PET/CT exhibited increased tumoral activity retention, along with elevated tumor-to-background uptake ratios, in comparison to ^{18}F-FDG PET/CT, across all lesion locations (13.22 ± 8.1 vs 3.43 ± 2.12; $P < 0.001$; $z = -3.621$). Furthermore, significantly increased ^{68}Ga-FAPI uptake (mean, 13.8 ± 5.1) was detected in primary tumoral lesions compared with ^{18}F-FDG uptake (mean, 3.9 ± 3.0; $P < 0.001$; $z = 3.621$) (Table 2; Figs. 3 and 4).

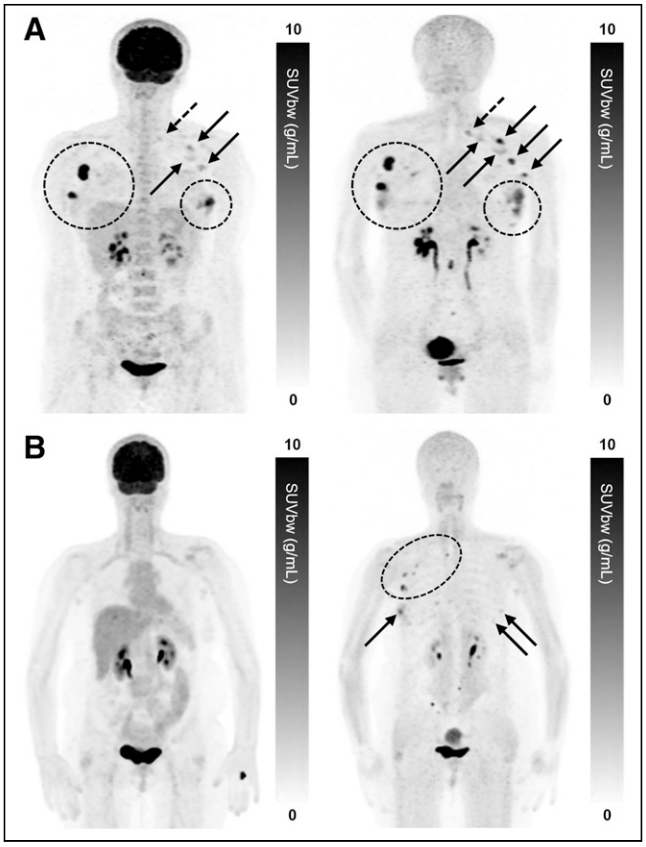

FIGURE 2. Maximum-intensity projection ^{18}F-FDG PET (left) and ^{68}Ga-FAPI PET (right) images of synchronous ILC. (A) 42-y-old patient with multicentric primary lesions (encircled), regional (solid arrows), and distant inferior jugular lymph node (dashed arrows) seen on ^{18}F-FDG PET and subsequently confirmed on ^{68}Ga-FAPI PET, which also revealed additional malignant foci aligned with MRI. Some lesions exhibited high activity retention on ^{68}Ga-FAPI PET. (B) 53-y-old patient showing no significant uptake on ^{18}F-FDG PET but synchronous bilateral lesions (arrows) on ^{68}Ga-FAPI PET, which also identified pathologic lymph nodes (encircled), resulting in upstaging. SUVbw = body-weight SUV.

TABLE 1
Clinical and Pathologic Features of Patients

Feature	Data
Mean age (y)	51 (range, 37–79)
Pathologic score	
5	2 (8.7)
6	6 (26.1)
7	7 (30.4)
8	3 (13,1)
9	5 (21.7)
Grade	
1	2 (8.7)
2	13 (56.5)
3	8 (34.8)
Mean ratio of tumor to stroma	0.91 (SD, 1.92)
Peritumoral lymphocyte infiltration	
Evident	6 (26.1)
Not evident	17 (73.9)
Molecular subtypes	
Luminal A	15 (65)
Luminal B/human epidermal growth factor receptor 2–negative	8 (35)
Primary surgery before scanning	
Yes	4 (17)
No	19 (83)
Premenopausal	8 (35)
Postmenopausal	15 (65)
Bilateral breast cancer	
Yes	2 (9)
No	21 (91)
Metastatic disease	
Yes	11 (47.8)
No	12 (52.2)

Qualitative data are number followed by percentage in parentheses.

Among the 23 patients, 19 had a primary breast lesion, whereas 4 had previously undergone mastectomy. Among those with a primary breast lesion, 6 had a solitary breast lesion, and 13 had multicentric breast cancer. The median size of primary breast lesions was 20.5 mm (range, 3–80 mm). In total, 44 breast lesions were analyzed, with only 2 lesions in the breast measuring less than 8 mm, indicating that all lesions were likely to be ^{18}F-FDG PET/CT–avid. Although the number of primary breast lesions detected was identical for both ^{18}F-FDG PET/CT and ^{68}Ga-FAPI PET/CT (25 lesions), ^{68}Ga-FAPI PET/CT identified an additional 19 foci (Table 3). Notably, among the 7 patients initially assessed as having solitary breast cancer based on ^{18}F-FDG PET/CT, ^{68}Ga-FAPI PET/CT revealed them to have multicentric breast cancer. Moreover, ^{68}Ga-FAPI PET/CT detected a higher number of multicentric foci in 3 patients. Additionally, 4 patients exhibited nonavid lesions in the contralateral breast on ^{18}F-FDG PET/CT that

TABLE 2
SUV_{max} of ^{18}F-FDG PET/CT and ^{68}Ga-FAPI PET/CT According to Lesion Location

Lesion location	SUV_{max}		*P**
	^{18}F-FDG PET/CT	^{68}Ga-FAPI PET/CT	
Primary breast	3.9 ± 3.0	13.8 ± 5.1	0.001
Local/distant lymph node metastasis	1.15 ± 0.8	11.5 ± 5.9	0.012
Liver metastasis†	1.73 ± 1.27	6,37 ± 3,5	None
Bone metastasis	5.3 ± 4.1	19.1 ± 6.0	0.017

*Wilcoxon signed-rank test.
†Number of lesions (n = 3) was found to be insufficient for meaningful statistical analysis.
Data are mean ± SD.

were detectable on ^{68}Ga-FAPI PET/CT. No correlation was observed between the size of primary breast lesions and either ^{18}F-FDG PET/CT uptake (P = 0.33; r = 0.151) or ^{68}Ga-FAPI PET/CT uptake (P = 0.19; r = 0.201), possibly because most lesions were 1 cm or larger, where ^{18}F-FDG sensitivity is already higher.

Axillary lymph node metastasis was detected in 1 patient with ^{18}F-FDG PET/CT and in 8 patients with ^{68}Ga-FAPI PET/CT. The mean uptake value of ^{68}Ga-FAPI PET/CT (11.5 ± 5.9) was significantly higher than that of ^{18}F-FDG PET/CT (1.15 ± 0.8; P = 0.012; z = 2.521) (Table 2; Figs. 2 and 3). In total, 134 lymph nodes were measured, with short diameters ranging from 5 to 18 mm. Among them, 89.5% had a short diameter of 8 mm or less. Both ^{18}F-FDG PET/CT and ^{68}Ga-FAPI PET/CT showed involvement in 6 lymph nodes (4.5%). ^{18}F-FDG PET/CT demonstrated no uptake in 34 lymph nodes, whereas ^{68}Ga-FAPI PET/CT exhibited uptake in 25.4% of these nodes. Ninety-four lymph nodes were classified as benign by both imaging modalities (70.1%). Of the 40 metastatic lymph nodes, 30 were at level 1, and the rest were at level 2. There was a strong positive correlation between lymph node short diameter and ^{18}F-FDG PET/CT uptake values (P < 0.001; r = 0.625), whereas higher accumulation on ^{68}Ga-FAPI PET/CT resulted in higher sensitivity, and these lesions suffered less from the partial-volume effect (P < 0.001; r = 0.319).

Regarding metastatic sites, in 18 of 23 (78.2%) patients ^{68}Ga-FAPI PET/CT identified new lesions not seen on ^{18}F-FDG PET/CT, including multifocal primary lesions within the breast, local or distant lymph nodes, bone, and liver (Table 3; Figs. 4 and 5). Although 1 distant lymph node metastasis was detected on ^{18}F-FDG PET/CT, ^{68}Ga-FAPI PET/CT revealed an additional 3 patients with distant lymph node metastasis (mean, 3.0 and 8.5 ± 2.8, respectively). Bone metastases were detected in 7 of 8 patients on ^{18}F-FDG PET/CT, and an additional patient with bone metastasis was identified using ^{68}Ga-FAPI PET/CT. The total number of bone metastases detected on ^{18}F-FDG PET/CT was 264, compared with 473 on ^{68}Ga-FAPI PET/CT (Table 3; Fig. 5). In 87.5% of patients, the number of bone metastases detected by ^{68}Ga-FAPI PET/CT was higher than that detected by ^{18}F-FDG PET/CT. The mean uptake of ^{68}Ga-FAPI PET/CT was 19.1 ± 6.0, whereas it was 5.3 ± 4.1 for ^{18}F-FDG PET/CT (P = 0.017; z = 2.380) (Table 2). Furthermore, 3 new solitary liver metastases, undetectable on ^{18}F-FDG PET/CT, were visualized using ^{68}Ga-FAPI PET/CT (mean, 6.37 ± 3.5) (Table 3; Fig. 4).

The TNM classification and staging of 23 patients were compared between 2 imaging modalities. T categories were assessed in 19 patients, with operated cases classified as Tx. Both modalities showed a similar distribution among T category groups (Tx, T1, T2, T3, and T4). N category variations were observed: ^{18}F-FDG PET/CT showed 88% N0, 8% N1, and 4% N3, whereas ^{68}Ga-FAPI PET/CT showed 52%, 44%, and 4%, respectively, with 36% upstaging in N0 cases. Both modalities had comparable results for the M category, but ^{68}Ga-FAPI PET/CT revealed a 13% upstaging rate, indicating its ability to detect additional metastatic lesions. Lastly, the anatomic stage group analysis revealed 1 case (4.4%) as stage IA, 11 cases (47.8%) as IIA, 1 case (4.4%) as IIB, 1 case (4.4%) as IIIB, and 9 cases (39.1%) as IV. The single case identified as IA on ^{18}F-FDG PET/CT was later identified as IIA on ^{68}Ga-FAPI PET/CT, also in line with the reference standard. Similarly, 3 of the cases identified as IIA, 1 case identified as IIB, and 2 cases identified as IIA were later upstaged by ^{68}Ga-FAPI PET/CT to IIB, IV, and IV, respectively (Table 4).

Correlation Analysis of Imaging Uptake Ratios and Pathologic Features

The mean uptake value in patients with luminal A disease was 4.42 ± 3.66 by ^{18}F-FDG PET/CT, whereas it was 2.44 ± 0.23 in the luminal B subgroup (P = 0.092). Correspondingly, these values were 13.6 ± 5.4 and 14.6 ± 5.7 by ^{68}Ga-FAPI PET/CT (P = 0.706). There was no correlation between the luminal A or B subgroup and the ratio of ^{18}F-FDG PET/CT to ^{68}Ga-FAPI PET/CT SUV_{max} (P = 0.102; r = −0.42).

Moreover, no significant correlation was found between the other pathologic features of tumor and the uptake ratio of ^{18}F-FDG to ^{68}Ga-FAPI PET/CT (glandular differentiation [r = 0.32; P = 0.17], nuclear polymorphism [r = 0.23; P = 0.34], mitosis count [r = 0.31; P = 0.18], grade score [r = 0.38; P = 0.099], grade [r = 0.19; P = 0.43], or tumor-to-stroma ratio [r = 0.29; P = 0.21]). In contrast, a moderately significant positive correlation was observed between the peritumoral lymphocyte ratio and the ^{68}Ga-FAPI PET/CT–to–^{18}F-FDG PET/CT SUV_{max} ratio (r = 0.498; P = 0.026). This suggests that a higher peritumoral lymphocyte ratio was associated with a higher uptake ratio of ^{68}Ga-FAPI PET/CT to ^{18}F-FDG PET/CT.

DISCUSSION

False-negative rates are higher for ILCs than for ductal breast cancers. Although MRI demonstrates high sensitivity in detecting

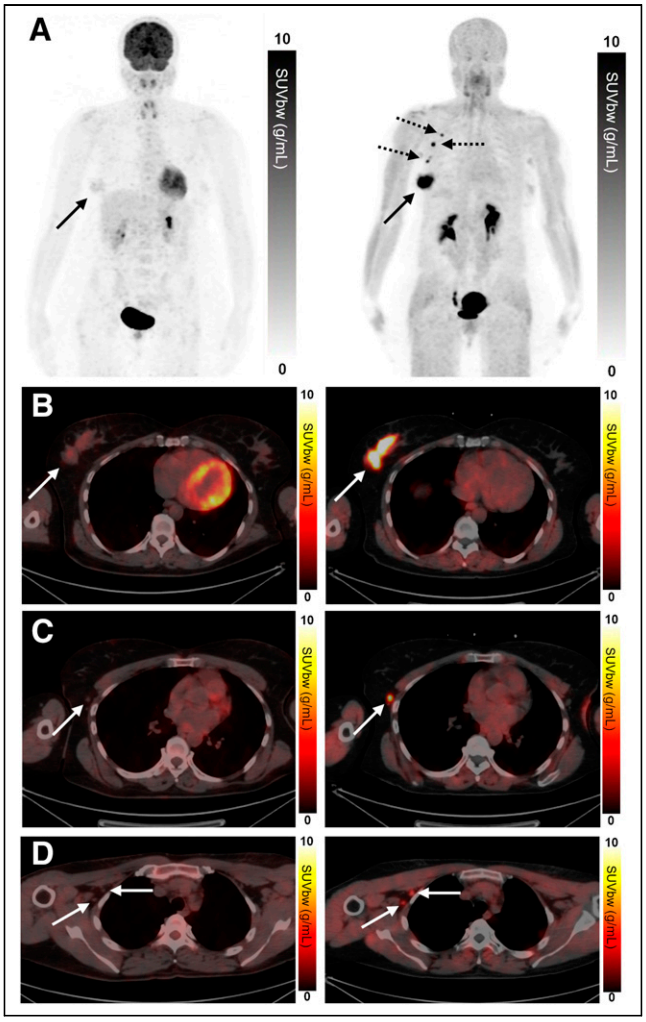

FIGURE 3. Maximum-intensity projection ^{18}F-FDG PET (left) and ^{68}Ga-FAPI PET (right) images (A) and axial hybrid ^{18}F-FDG PET/CT (left) and ^{68}Ga-FAPI PET/CT (right) images (B–D) of 50-y-old patient with right bifocal ILC. (A and B) Two adjacent breast lesions with low ^{18}F-FDG PET/CT uptake showed significantly higher uptake on ^{68}Ga-FAPI PET/CT (solid arrows). Dashed arrows in right panel indicate regional lymph nodes detected by FAPI PET/CT. (C and D) Axillary lymph nodes (arrows) without activity on ^{18}F-FDG PET/CT exhibited significant uptake on ^{68}Ga-FAPI PET/CT, leading to upstaging in N category. SUVbw = body-weight SUV.

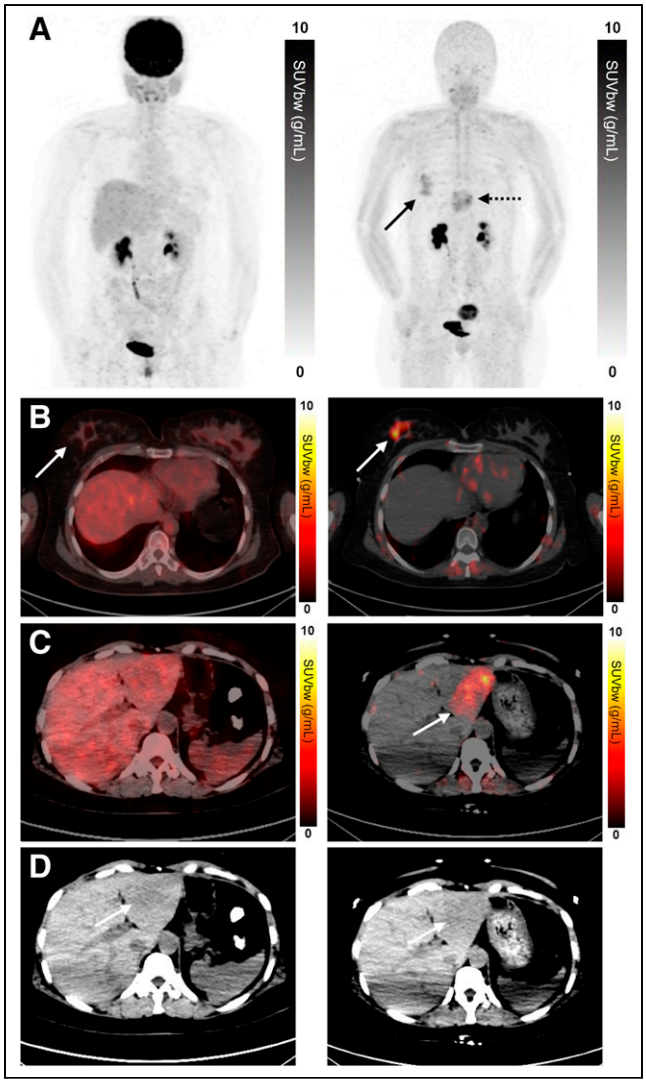

FIGURE 4. Maximum-intensity projection ^{18}F-FDG PET (left) and ^{68}Ga-FAPI PET (right) images (A), axial hybrid ^{18}F-FDG PET/CT (left) and ^{68}Ga-FAPI PET/CT (right) images (B and C), and axial CT images (D) of 42-y-old patient with right ILC. (A and B) Although ^{18}F-FDG PET/CT showed no significant activity in right breast lesion (white arrows), ^{68}Ga-FAPI PET/CT revealed substantial uptake. Dashed arrow in right panel A indicates liver lesion, whereas solid arrow indicates primary lesion. (C and D) In addition, liver lesion with vague borders on CT images (arrows) had no significant ^{18}F-FDG uptake but exhibited high ^{68}Ga-FAPI uptake, confirmed as breast cancer metastasis through MRI, indicating stage IV disease. SUVbw = body-weight SUV.

primary breast masses and axillary lymph nodes, ^{18}F-FDG PET serves as the most valuable tool for identifying distant metastases. In the presence of ILC, a secondary imaging method becomes necessary. Given that the stroma volume can surpass that of neoplastic cells, ^{68}Ga FAPI PET/CT appears to offer greater sensitivity than ^{18}F-FDG PET/CT, especially for detecting small lesions or those with low or heterogeneous glucose metabolism.

The limited sensitivity of ^{18}F-FDG PET/CT may be attributed not only to the low-grade nature of ILC but also to its pathogenetic characteristics. E-cadherin, a calcium-dependent transmembrane protein responsible for maintaining tissue integrity and cell-to-cell adhesion while preventing tissue invasion (*29*), is absent in approximately 85% of cases of ILC. This absence leads to a loss of adhesion proteins and disrupts the morphologic pattern, resulting in tumor cells that are individually dispersed or arranged in a single-file pattern, loosely distributed throughout a fibrous matrix with minimal desmoplastic response (*30*). Additionally, the tumor-infiltrating lymphocyte rate is typically low. Theoretically, the unique nature of ILC may reduce the sensitivity of ^{18}F-FDG PET/CT because of the dispersion of glucose-intensive tumor tissue; however, this may not affect the effectiveness of ^{68}Ga-FAPI PET/CT.

Although the benefits of ^{68}Ga-FAPI PET/CT have been demonstrated in numerous studies involving small patient cohorts (*31*), it is not yet routinely recommended by national guidelines because of the lack of high-level evidence. Initially, Kömek et al. conducted a prospective study on 20 patients with breast cancer, demonstrating that the sensitivity and specificity of ^{68}Ga-FAPI PET/CT in detecting primary breast lesions were 100% and 95.6%, respectively. In comparison, the sensitivity and specificity of ^{18}F-FDG PET/CT were 78.2% and 100%, respectively (*25*).

TABLE 3
Comparison of Lesion Number on ^{18}F-FDG PET/CT and ^{68}Ga-FAPI PET/CT According to Location

Lesion location	New malignant lesions*	Coherent malignant lesions†	Benign lesions‡	Total lesions	
				^{18}F-FDG PET/CT	^{68}Ga-FAPI PET/CT
Primary breast	19	25	0	25	34
Local/distant lymph node metastasis	34	6	94	100	134
Liver metastasis	3	0	0	0	3
Bone metastasis	209	264	0	264	473
Total	265	295	94	389	644

*Number of new malignant lesions detected on ^{68}Ga-FAPI PET/CT in line with reference standard.
†Number of malignant lesions detected on both PET/CT modalities in line with reference standard.
‡Number of lesions detected on both PET/CT modalities and concluded to be benign according to reference standard.

Subsequently, Elboga et al. conducted a retrospective study on 48 invasive breast cancer patients, revealing that ^{68}Ga-FAPI PET/CT detected a higher number of primary breast lesions and new metastatic lesions with higher uptake values than did ^{18}F-FDG PET/CT (*26*). The effectiveness of ^{18}F-FDG PET/CT was decreasing, especially in the ILC subtype, highlighting the need for a more effective imaging method, particularly in this patient group. In a prospective study by Alçın et al., which included 11 cases of ILC (*32*), patients with low avidity as determined by ^{18}F-FDG PET/CT scans were examined. The study found that ^{68}Ga-FAPI PET/CT yielded higher sensitivity and higher SUV_{max} than did ^{18}F-FDG PET/CT in breast cancer patients with low ^{18}F-FDG affinity. Additionally, ^{68}Ga-FAPI PET/CT identified additional lesions in the primary region, lymph nodes, and 1 lung metastatic nodule. Another prospective pilot trial involving 7 ILC patients with disease that was not ^{18}F-FDG–avid indicated that ^{68}Ga-FAPI PET/CT detected an increased number of lesions compared with CT alone ($P = 0.022$) (*27*).

Examining these studies reveals a lack of specificity and limited patient numbers within the ILC subgroup. Therefore, our retrospective study comparing ^{68}Ga-FAPI PET/CT with ^{18}F-FDG PET/CT in ILC patients holds significance for data accumulation and knowledge expansion. With a larger patient cohort than other studies, our findings show that ^{68}Ga-FAPI PET/CT detected more lesions and exhibited high tumor-to-background uptake ratios. Regardless of pathologic features, new lesions in the primary breast, local or distant lymph nodes, bone, and liver were found in 73.9% of patients using ^{68}Ga-FAPI PET/CT compared with ^{18}F-FDG PET/CT.

We studied 44 breast lesions, with only 2 having a size less than 8 mm. Although all lesions likely showed ^{18}F-FDG PET/CT uptake

TABLE 4
Comparison of TNM Classifications and Anatomic Stage Groups Between 2 Modalities

Category	Stage	^{18}F-FDG PET/CT	^{68}Ga-FAPI PET/CT	Upstaging
T ($n = 25$)	T1	4 (16.0)	4 (16.0)	0
	T2	15 (60.0)	15 (60.0)	
	T3	1 (4.0)	1 (4.0)	
	T4	1 (4.0)	1 (4.0)	
	Tx	4(16.0)	4 (16.0)	
N ($n = 25$)	N0	22 (88.0)	13 (52.0)	9 (36.0)
	N1	2 (8.0)	11 (44.0)	
	N3	1 (4.0)	1 (4.0)	
M ($n = 23$)	M0	14 (60.9)	11 (47.8)	3 (13.0)
	M1	9 (39.1)	12 (52.2)	
Anatomic stage group ($n = 23$)	IA	1 (4.4)	0	7 (30.4)
	IIA	11 (47.8)	7 (30.4)	
	IIB	1 (4.4)	3 (13.0)	
	IIIB	1 (4.4)	1 (4.4)	
	IV	9 (39.1)	12 (52.2)	

Data are number followed by percentage in parentheses.

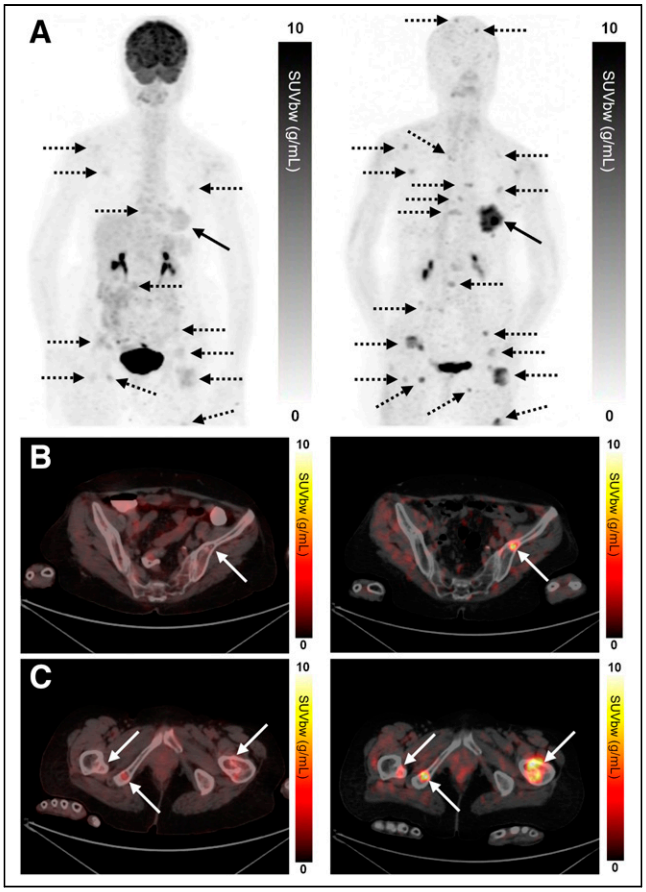

FIGURE 5. Maximum-intensity projection ^{18}F-FDG PET (left) and ^{68}Ga-FAPI PET (right) images (A) and axial hybrid ^{18}F-FDG PET/CT (left) and ^{68}Ga-FAPI PET/CT (right) images (B and C) of 68-y-old patient with left ILC. (A and B) Notable difference in uptake between ^{18}F-FDG PET/CT and ^{68}Ga-FAPI PET/CT was observed in left breast lesion (solid arrow). Multiple disseminated focal uptakes (dashed arrows) corresponding to predominantly ^{68}Ga-FAPI–avid bone lesions were detected, including in calvarium and vertebral column. (B and C) Most bone lesions (arrows) showed osteolytic features in both ^{18}F-FDG PET/CT and ^{68}Ga-FAPI PET/CT, with high ^{68}Ga-FAPI avidity. SUVbw = body-weight SUV.

regardless of size, ^{68}Ga-FAPI PET/CT identified 19 additional foci. MRI is more specific for primary breast lesions; however, ^{68}Ga-FAPI PET/CT, though not a replacement, has demonstrated superiority over ^{18}F-FDG PET/CT in previous studies.

Both ^{18}F-FDG PET/CT and ^{68}Ga-FAPI PET/CT consistently assessed tumor sizes in various T categories, showing agreement in primary tumor evaluation. Despite differences in N category analysis, ^{68}Ga-FAPI PET/CT exhibited higher sensitivity, leading to a 36% upstaging from N0 cases initially identified by ^{18}F-FDG PET/CT. Although overall M category results were comparable, ^{68}Ga-FAPI PET/CT revealed a 13% upstaging rate, detecting additional metastatic lesions. This has significant implications for treatment planning and prognosis assessment. Anatomic stage group analysis highlighted nuanced diagnostic capabilities, especially reclassifying regional diseases from stage III to IV in ^{68}Ga-FAPI PET/CT compared with ^{18}F-FDG PET/CT.

In our study a moderately significant positive correlation was identified between the peritumoral lymphocyte ratio and the ratio of ^{68}Ga-FAPI PET/CT to ^{18}F-FDG PET/CT ($r = 0.498$; $P = 0.026$). In a translational study conducted by Costa et al. (*33*), distinct subsets of CAFs within breast cancer were identified and labeled as CAF-S1 through CAF-S4, and CAF-S1 fibroblasts were associated with the infiltration of FOXP3+ T lymphocytes in breast cancer cases. In line with these findings, the observed correlation between peritumoral lymphocyte infiltration and FAPI involvement suggests that this connection could potentially serve as an indicative measure of FAP's function within immune modulation.

In addition to its success in detecting primary lesions, ^{68}Ga-FAPI PET/CT also excelled in detecting lymph node uptake. Our study showed that ^{68}Ga-FAPI PET/CT identifies axillary lymph node metastases more effectively than ^{18}F-FDG PET/CT does. Despite morphologic suspicions in ^{18}F-FDG PET/CT, 89.5% of nodes with a short diameter of 8 mm or less did not exhibit ^{18}F-FDG uptake. Unlike ^{18}F-FDG, ^{68}Ga-FAPI uptake displayed a weak correlation with lymph node size, suggesting size-independent uptake.

Consistent with the studies mentioned previously, ^{68}Ga-FAPI PET/CT appeared to be superior to ^{18}F-FDG PET/CT in detecting distant metastases in our study (*25–27*,*32*).

Eshet et al. conducted a prospective pilot trial that indicated that ^{68}Ga-FAPI PET/CT detected more lesions than CT alone ($P = 0.022$) in 7 ILC patients whose disease was not ^{18}F-FDG–avid (*27*). A notable aspect of this study is that metastatic or progressing sites were poorly demonstrated not only by ^{18}F-FDG PET/CT but also by conventional CT and bone scans. This suggests that secondary imaging methods may be inadequate for recognizing the ILC subtype. Furthermore, in this case series, ^{68}Ga-FAPI PET/CT revealed more extensive skeletal disease, aligning with our findings.

In the present study, the number of bone metastases was increased on ^{68}Ga-FAPI PET/CT compared with ^{18}F-FDG PET/CT in 7 of 8 patients (87.5%). The mean ^{68}Ga-FAPI uptake for bone metastasis was significantly higher than the mean ^{18}F-FDG uptake ($P = 0.017$; $z = 2.380$).

We found 3 liver metastases missed by ^{18}F-FDG PET/CT but detectable with ^{68}Ga-FAPI PET/CT. Building on our previous research (*26*), we argue that ^{68}Ga-FAPI PET/CT, with its low liver background activity, enhances liver metastasis detection, evident in the high tumor-to-background uptake ratios.

Despite ^{68}Ga-FAPI PET/CT's capability to reveal new breast lesions, their significance should be confirmed histopathologically or considered primary on the basis of MRI results. The primary value of ^{68}Ga-FAPI PET/CT lies in detecting regional lymph node and distant metastases, especially when other imaging modalities such as ultrasound, CT, and bone scintigraphy may be insufficient for primary breast lesions.

There are limited studies, as mentioned earlier, comparing ^{68}Ga-FAPI PET/CT and ^{18}F-FDG PET/CT head to head, and these studies include only a low number of ILC patients (*27*,*32*). Our study, with the highest number of ILC cases to our knowledge, offers a comprehensive comparison between ^{18}F-FDG and ^{68}Ga-FAPI PET/CT, making a unique contribution to the literature. It highlights the ability of ^{68}Ga-FAPI PET/CT to lower false-negative rates compared with ^{18}F-FDG PET/CT.

Although our case number was relatively high compared with the limited studies on this subject in the literature, our main limitation is the relatively low case count. Other important limitations include the lack of a prospective randomized study design and the absence of histopathologic confirmation for all metastatic lesions, excluding primary breast lesions and target lesions.

CONCLUSION

Our study contributes to the evidence supporting ^{68}Ga-FAPI PET/CT's utility in ILC, including staging. Nuanced differences, especially in lymph node involvement and metastatic lesion detection, underscore its complementary role with ^{18}F-FDG PET/CT. These insights can inform clinical decisions, providing a more comprehensive understanding of disease extent and refining treatment strategies for breast cancer patients. Larger-cohort studies are needed to validate and build on these initial findings.

DISCLOSURE

No potential conflict of interest relevant to this article was reported.

KEY POINTS

QUESTION: Is ^{68}Ga-FAPI PET/CT a more useful imaging method than ^{18}F-FDG PET/CT in ILC?

PERTINENT FINDINGS: In this cohort study examining 23 women with ILC, ^{68}Ga-FAPI PET/CT appeared to be superior to ^{18}F-FDG PET/CT in showing the primary lesion and metastases of the lymph nodes and other organs.

IMPLICATIONS FOR PATIENT CARE: ^{68}Ga-FAPI PET/CT might become a viable alternative to ^{18}F-FDG PET/CT based on the outcomes of future studies involving larger patient cohorts.

REFERENCES

1. Ferlay J, Soerjomataram I, Dikshit R, et al. Cancer incidence and mortality worldwide: sources, methods and major patterns in GLOBOCAN 2012. *Int J Cancer.* 2015;136:E359–E386.
2. Li CI, Anderson BO, Daling JR, et al. Trends in incidence rates of invasive lobular and ductal breast carcinoma. *JAMA.* 2003;289:1421–1424.
3. Li CI, Daling JR. Changes in breast cancer incidence rates in the United States by histologic subtype and race/ethnicity, 1995 to 2004. *Cancer Epidemiol Biomarkers Prev.* 2007;16:2773–2780.
4. Siegel RL, Miller KD, Jemal A. Cancer statistics, 2018. *CA Cancer J Clin.* 2018; 68:7–30.
5. Goetz MP, Gradishar WJ, Anderson BO, et al. NCCN guidelines insights: breast cancer version, 3.2018. *J Natl Compr Canc Netw.* 2019;17:118–126.
6. Lebron-Zapata L, Jochelson MS. Overview of breast cancer screening and diagnosis. *PET Clin.* 2018;13:301–323.
7. Kitajima K, Miyoshi Y. Present and future role of FDG-PET/CT imaging in the management of breast cancer. *Jpn J Radiol.* 2016;34:167–180.
8. Hogan MP, Goldman DA, Dashevsky B, et al. Comparison of ^{18}F-FDG PET/CT for systemic staging of newly diagnosed invasive lobular carcinoma versus invasive ductal carcinoma. *J Nucl Med.* 2015;56:1674–1680.
9. Borst MJ, Ingold JA. Metastatic patterns of invasive lobular versus invasive ductal carcinoma of the breast. *Surgery.* 1993;114:637–641.
10. Kumar R, Chauhan A, Zhuang H, et al. Clinicopathologic factors associated with false negative FDG-PET in primary breast cancer. *Breast Cancer Res Treat.* 2006; 98:267–274.
11. Avril N, Rose CA, Schelling M, et al. Breast imaging with positron emission tomography and fluorine-18 fluorodeoxyglucose: use and limitations. *J Clin Oncol.* 2000;18:3495–3502.
12. McCart Reed AE, Kutasovic JR, Lakhani SR, Simpson PT. Invasive lobular carcinoma of the breast: morphology, biomarkers and 'omics. *Breast Cancer Res.* 2015;17:12.
13. Ulaner GA, Jhaveri K, Chandarlapaty S, et al. Head-to-head evaluation of ^{18}F-FES and ^{18}F-FDG PET/CT in metastatic invasive lobular breast cancer. *J Nucl Med.* 2021;62:326–331.
14. Kurland BF, Peterson LM, Lee JH, et al. Estrogen receptor binding (^{18}F-FES PET) and glycolytic activity (^{18}F-FDG PET) predict progression-free survival on endocrine therapy in patients with ER+ breast cancer. *Clin Cancer Res.* 2017;23:407–415.
15. Siveke JT. Fibroblast-activating protein: targeting the roots of the tumor microenvironment. *J Nucl Med.* 2018;59:1412–1414.
16. Garin-Chesa P, Old LJ, Rettig WJ. Cell surface glycoprotein of reactive stromal fibroblasts as a potential antibody target in human epithelial cancers. *Proc Natl Acad Sci USA.* 1990;87:7235–7239.
17. Hamson EJ, Keane FM, Tholen S, Schilling O, Gorrell MD. Understanding fibroblast activation protein (FAP): substrates, activities, expression and targeting for cancer therapy. *Proteomics Clin Appl.* 2014;8:454–463.
18. Jansen K, Heirbaut L, Cheng JD, et al. Selective inhibitors of fibroblast activation protein (FAP) with a (4-quinolinoyl)-glycyl-2-cyanopyrrolidine scaffold. *ACS Med Chem Lett.* 2013;4:491–496.
19. Loktev A, Lindner T, Mier W, et al. A tumor-imaging method targeting cancer associated fibroblasts. *J Nucl Med.* 2018;59:1423–1429.
20. Lindner T, Loktev A, Altmann A, et al. Development of quinoline-based theranostic ligands for the targeting of fibroblast activation protein. *J Nucl Med.* 2018;59: 1415–1422.
21. Giesel FL, Kratochwil C, Lindner T, et al. ^{68}Ga-FAPI PET/CT: biodistribution and preliminary dosimetry estimate of 2 DOTA-containing FAP-targeting agents in patients with various cancers. *J Nucl Med.* 2019;60:386–392.
22. Kratochwil C, Flechsig P, Lindner T, et al. ^{68}Ga-FAPI PET/CT: tracer uptake in 28 different kinds of cancer. *J Nucl Med.* 2019;60:801–805.
23. Scanlan MJ, Raj BK, Calvo B, et al. Molecular cloning of fibroblast activation protein alpha, a member of the serine protease family selectively expressed in stromal fibroblasts of epithelial cancers. *Proc Natl Acad Sci USA.* 1994;91:5657–5661.
24. Šimková A, Busek P, Sedo A, Konvalinka J. Molecular recognition of fibroblast activation protein for diagnostic and therapeutic applications. *Biochim Biophys Acta Proteins Proteomics.* 2020;1868:140409.
25. Kömek H, Can C, Güzel Y, et al. ^{68}Ga-FAPI-04 PET/CT, a new step in breast cancer imaging: a comparative pilot study with the ^{18}F-FDG PET/CT. *Ann Nucl Med.* 2021;35:744–752.
26. Elboga U, Sahin E, Kus T, et al. Superiority of ^{68}Ga-FAPI PET/CT scan in detecting additional lesions compared to ^{18}FDG PET/CT scan in breast cancer. *Ann Nucl Med.* 2021;35:1321–1331.
27. Eshet Y, Tau N, Apter S, et al. The role of ^{68}Ga-FAPI PET/CT in detection of metastatic lobular breast cancer. *Clin Nucl Med.* 2023;48:228–232.
28. *AJCC Cancer Staging Manual.* Springer International Publishing; 2017:589–636.
29. Vleminckx K, Vakaet L Jr, Mareel M, Fiers W, Van Roy F. Genetic manipulation of E-cadherin expression by epithelial tumor cells reveals an invasion suppressor role. *Cell.* 1991;66:107–119.
30. Thomas M, Kelly ED, Abraham J, Kruse M. Invasive lobular breast cancer: a review of pathogenesis, diagnosis, management, and future directions of early stage disease. *Semin Oncol.* 2019;46:121–132.
31. Wass G, Clifford K, Subramaniam RM. Evaluation of the diagnostic accuracy of FAPI PET/CT in oncologic studies: systematic review and metaanalysis. *J Nucl Med.* 2023;64:1218–1224.
32. Alçın G, Arslan E, Aksoy T. ^{68}Ga-FAPI-04 PET/CT in selected breast cancer patients with low FDG affinity a head-to-head comparative study. *Clin Nucl Med.* 2023;48:e420–e430.
33. Costa A, Kieffer Y, Scholer-Dahirel A, et al. Fibroblast heterogeneity and immunosuppressive environment in human breast cancer. *Cancer Cell.* 2018;33:463–479.e10.